Reachability-based Trajectory Optimization for Robotic Systems Given Sequences of Rigid Contacts

Conference Paper · July 2020

DOI: 10.23919/ACC45564.2020.9147926

4 authors:

Jaemin Lee
University of Texas at Austin
21 PUBLICATIONS **138** CITATIONS
SEE PROFILE

Junhyeok Ahn
University of Texas at Austin
13 PUBLICATIONS **38** CITATIONS
SEE PROFILE

Efstathios Bakolas
University of Texas at Austin
85 PUBLICATIONS **787** CITATIONS
SEE PROFILE

Luis Sentis
University of Texas at Austin
152 PUBLICATIONS **2,824** CITATIONS
SEE PROFILE

Reachability-based Trajectory Optimization for Robotic Systems Given Sequences of Rigid Contacts

Jaemin Lee[1], Junhyeok Ahn[1], Efstathios Bakolas[2], and Luis Sentis[2]

Abstract— **This paper proposes a method to generate feasible trajectories for robotic systems with predefined sequences of switched contacts. The proposed trajectory generation method relies on sampling-based methods, optimal control, and reachability analysis. In particular, the proposed method is able to quickly test whether a simplified model-based planner, such as the Time-to-Velocity-Reversal planner, provides a reachable contact location based on reachability analysis of the multi-body robot system. When the contact location is reachable, we generate a feasible trajectory to change the contact mode of the robotic system smoothly. To perform reachability analysis efficiently, we devise a method to compute forward and backward reachable sets based on element-wise optimization over a finite time horizon. Then, we compute robot trajectories by employing optimal control. The main contributions of this study are the following. Firstly, we guarantee whether planned contact locations via simplified models are feasible by the robot system. Secondly, we generate optimal trajectories subject to various constraints given a feasible contact sequence. Lastly, we improve the efficiency of computing reachable sets for a class of constrained nonlinear systems by incorporating bi-directional propagation (forward and backward). To validate our methods we perform numerical simulations applied to a humanoid robot walking.**

I. INTRODUCTION

Many intelligent robot systems physically interact with the environment or other agents through rigid contacts using their end-effectors. For instance, to achieve dynamic legged locomotion, Grizzle et al. introduce a hybrid zero dynamics approach and proposed a feedback controller that guarantees periodic locomotion [1]. Zhao et al. propose a motion planning method for non-periodic locomotion based on a phase space hybrid model and Centroidal Dynamics (CD) [2]. In robotic manipulation, hybrid control is employed when the robot interacts with the environment using position-force trajectories [3]. Similar to these studies, the methods considered here aim to enable robots to interact with their environment with contact transitions and while dealing with complex robot constraints.

In particular, this study aims to generate a feasible trajectory for robotic systems with rigid contacts that have friction cone constraints. Optimal control theory has been utilized to solve similar problems. For instance, the unconstrained iterative Linear Quadratic Regulation (iLQR) algorithm has been utilized to generate trajectories considering contacts [4]–[6]. iLQR-based methods solve the trajectory generation problem through contacts faster than nonlinear optimization methods. However, the results may not strictly satisfy all constraints because of the reliance on linearization and convexification. Posa et al. proposed an approach to directly solve the nonlinear optimization problem of rigid bodies with contacts, leveraging Sequential Quadratic Programming (SQP) [7]. Although this SQP-based method provides a solution satisfying contact constraints, significant computation time is required to solve the nonlinear program (NLP). To improve the performance of these types of NLP optimization problems, our previous work proposed an approach combining optimization-based reachability with direct trajectory optimization [8]. In this study, we aim to extend our previous method for generating an optimal trajectory for robotic systems with multi-body dynamics, complex constraints, and switched contacts.

In humanoids, the planning process typically relies on simplified models, such as the Linear Inverted Pendulum Model (LIPM) [9]–[13], and computes contact locations based on Center of Mass (CoM) dynamic behavior. For instance, the Time-to-Velocity-Reversal (TVR) planner computes the next contact location using the LIPM [11]. Kim et al. interpolate trajectories of the robot end-effectors based on planned contact locations. The robot then tracks those trajectories using a Whole Body Controller (WBC) [14]. Dai et al. use CD and full-body kinematics for trajectory calculations [12]. For a quadruped robot, the CD method is convexified to generate locomotion trajectories. After checking the friction cone stability margin, robots are controlled to follow the planned motions using a WBC [13]. Since these methods rely on simple models, they often result in trajectories that are not feasible by the robot system. Different from this, our work uses complex multi-body models that capture more closely the robot dynamics to check for contact feasibility and recompute unfeasible contact locations.

In optimal control theory, reachability analysis has been widely studied to obtain optimal and safe trajectories, for instance forward reachability has been used in [15]. In [16], forward Reachable Sets (FWR) are efficiently constructed using zonotopes in linear systems. However, this FWR cannot be applied to nonlinear and hybrid dynamical systems. Backward reachability analysis has been used to compute safe trajectories via Hamilton-Jacobi (HJ) PDEs [17], [18]. HJ PDE-based reachability analysis has been used to design feedback linearizing controller for simple systems [19], but

This work was supported by an NSF Grant# 1724360 and partially supported by an ONR Grant# N000141512507. The third author acknowledges partial support by NSF under Grant #1924790.

[1] J. Lee and J. Ahn are with the Department of Mechanical Engineering, The University of Texas at Austin, TX, 78712, USA {jmlee87, junhyeokahn91}@utexas.edu

[2] E. Bakolas and L. Sentis are with the Department of Aerospace Engineering and Engineering Mechanics, The University of Texas at Austin, TX, 78712, USA {bakolas, lsentis}@austin.utexas.edu

it is still not suitable for systems with high dimensionality. In addition, it is difficult to formulate our problem using HJ PDEs. Alternatively, sampling techniques have been employed to efficiently obtain reachable sets. In [20], a sampling-based approximation is utilized to perform reachability analysis given user-defined accuracy specifications. Our previous work proposed an efficient method to obtain reachable sets by combining sampling-based techniques and Quadratic Programming (QP) [8], [21].

This paper leverages sampling-based techniques and QPs to obtain forward and backward reachable sets. We previously used a simpler version of this method consisting only on forward reachability in [8]. We now propose a new approach to obtain backward reachable sets. Our proposed method is much more efficient than NLP. For efficiency, we check for contact feasibility during contact transitions. After contact locations are validated by our reachability method, we formulate an Optimal Control Problem (OCP) to find feasible trajectories satisfying state, input, and Contact Wrench Cone (CWC) constraints [22]. Putting everything together we achieve dynamic legged locomotion with optimal trajectories for humanoid robot systems.

To the best of our knowledge, this is the first study to integrate TVR contact planning and reachability-based trajectory generation. The main contributions are as follows. Firstly, our approach efficiently checks whether planned contact locations are feasible based on robot multi-body dynamics. Secondly, our method generates optimal and feasible state trajectories strictly fulfilling realistic physical constraints. The last contribution is the improved computational efficiency during reachability analysis. We reduce computational time by propagating robot states in a bidirectional manner.

The remainder of this paper is organized as follows. Notations, robotic systems with contact forces, constraints, and our problem definition are explained in Section II. In Section III, we briefly recall the TVR planner and detail the process for solving the problem of checking for kinematic feasibility, identifying reachable sets in the discrete-time domain, and solving the OCP. Section IV provides simulation results to show the efficiency of the proposed algorithm and presents a comparative analysis with our previous method.

II. PRELIMINARIES

A. Notation

The set of real n-dimensional vectors and $n \times m$ matrices are denoted by $\mathbb{R}^n$ and $\mathbb{R}^{n\times m}$, respectively. We represent the set of positive definite matrices and positive semi-definite matrices by $\mathbb{S}^n_{>0}$ and $\mathbb{S}^n_{\geq 0}$, respectively. We denote by $\mathrm{vertcat}(\mathbf{A}_1, \cdots, \mathbf{A}_k)$ the block matrix that results by vertically concatenating the matrices $\mathbf{A}_1, \cdots, \mathbf{A}_k$ which have the same number of columns. Given a matrix $\mathbf{A} \in \mathbb{R}^{n\times m}$ where $n \leq m$ and $\mathrm{rank}(\mathbf{A}\mathbf{A}^\top) = n$, we denote by $\mathbf{A}^\dagger$ the pseudo-inverse of $\mathbf{A}$, that is, $\mathbf{A}^\dagger := \mathbf{A}^\top \left(\mathbf{A}\mathbf{A}^\top\right)^{-1}$. In addition, $\mathbf{A}^{\dagger\mathbf{B}}$ denotes the pseudo-inverse of $\mathbf{A}$ weighted by $\mathbf{B}$ where $\mathbf{B} \in \mathbb{S}^m_{>0}$, that is $\mathbf{A}^{\dagger\mathbf{B}} := \mathbf{B}\mathbf{A}^\top \left(\mathbf{A}\mathbf{B}\mathbf{A}^\top\right)^{-1}$. Suppose that $a \in \mathbb{R}^n$ and $\mathbf{A} \in \mathbb{S}^n_{>0}$ be given, then $\|a\|_\mathbf{A} := \sqrt{a^\top \mathbf{A} a}$ denotes a weighted vector norm of a. Given two sets $\mathcal{A}$, $\mathcal{B} \subseteq \mathbb{R}^n$, then we denote by $\mathcal{A}\backslash\mathcal{B} \subseteq \mathbb{R}^n$ the complement of $\mathcal{A}$ with respect to $\mathcal{B}$.

B. System Description

Given a set of contact indices, $\mathcal{I}$, the rigid-body dynamics equation of the robotic systems exerted by the contact forces is described as

$$\mathbf{M}(q)\ddot{q} + b(\dot{q}, q) = \mathbf{S}^\top u + \sum_{i\in\mathcal{I}} \mathbf{J}_{c,i}^\top(q)\lambda_{c,i} \tag{1}$$

where $\mathbf{M}(q) \in \mathbb{S}^{n_q}_{>0}$, $b(\dot{q}, q) \in \mathbb{R}^{n_q}$, $\mathbf{S} \in \mathbb{R}^{n_u \times n_q}$, $u \in \mathbb{R}^{n_u}$, $\lambda_{c,i} \in \mathbb{R}^6$, and $\mathbf{J}_{c,i}(q) \in \mathbb{R}^{6\times n_q}$ denote the mass/inertia matrix, sum of Coriolis/centrifugal and gravitational forces, selection matrix for actuators, input command, i-th contact wrench, and the corresponding Jacobian, respectively. In addition, q, $\dot{q}$, and $\ddot{q}$ represent the joint position, velocity and acceleration of the robotic system. We consider $\mathbf{M}$, b, and $\mathbf{J}$ as $\mathbf{M}(q)$, $b(q, \dot{q})$, and $\mathbf{J}(q)$, respectively. Suppose $x = [q^\top, \dot{q}^\top]^\top \in \mathcal{X}$ be the system state then the continuous-time state model of the system becomes

$$\begin{aligned} \dot{x} &= \begin{bmatrix} \dot{q} \\ \mathbf{M}^{-1}\left(\mathbf{S}^\top u + \sum_{i\in\mathcal{I}} \mathbf{J}_{c,i}^\top \lambda_{c,i} - b\right) \end{bmatrix} \\ &= f(x, u, m, \lambda_c) \end{aligned} \tag{2}$$

where $m \in \mathcal{M}$ is a contact mode of the robots and $\lambda_c = \mathrm{vertcat}(\lambda_{c,i}, \forall i \in \mathcal{I}_m)$ is the stack of contact wrenches with respect to the mode m.

We assume that the output of the system is a function of the state as follows :

$$y(t) = f_y(x(t)) \tag{3}$$

where $f_y : \mathbb{R}^{n_x} \mapsto \mathbb{R}^{n_y}$ is continuous. The system dynamics, f, and the output function, f_y, are Lipschitz continuous in x. Typically, the output of a robotic system lies in a nonlinear manifold embedded in a high dimensional Euclidean space such as the manifold of positions and orientations of a robot's (rigid) body which is associated with the special Euclidean group $\mathrm{SE}(3)$.

C. Constraints

The robotic system is subject to the following state and input constraints:

$$h_{\mathrm{state}}(x) \leq 0, \quad h_{\mathrm{input}}(u) \leq 0 \tag{4}$$

where $h_{\mathrm{state}} : \mathbb{R}^{n_x} \mapsto \mathbb{R}^{n_{cs}}$ and $h_{\mathrm{input}} : \mathbb{R}^{n_u} \mapsto \mathbb{R}^{n_{ci}}$ denote continuous functions of the state and input constraints, respectively. The contact constraints make the problem more complicated and difficult. Suppose the mode m_k is given. The kinematic constraints for the rigid contacts are formulated as follows:

$$\begin{aligned} \phi_i(q) &= 0 \\ \dot{\phi}_i(q, \dot{q}) &= \frac{d\phi_r}{dt} = \mathbf{J}_{\phi_i}(q)\dot{q} = 0 \\ \ddot{\phi}_i(q, \dot{q}, \ddot{q}) &= \frac{d^2\phi_i}{dt^2} = \frac{d\mathbf{J}_{\phi_i}(q)}{dt}\dot{q} + \mathbf{J}_{\phi_i}(q)\ddot{q} = 0 \end{aligned} \tag{5}$$

where $i \in \mathcal{I}_{m_k}$ and $\phi_i : \mathbb{R}^{n_q} \mapsto \mathbb{R}^6$ denotes a continuous mapping for position and orientation errors of the i-th body with respect to the planned contact location. The time derivatives of $\phi_i(q)$ also have to vanish.

We also consider the CWC described in [22] to account for non-slip and non-flip contact constraints. Let us consider the contact wrench in the contact frame:

$$\lambda_{c,i}^{\text{local}} = \left[\begin{array}{cc} \mathbf{R}_{c,i}^\top(q) & \mathbf{0} \\ \mathbf{0} & \mathbf{R}_{c,i}^\top(q) \end{array} \right] \lambda_{c,i} \tag{6}$$

where $\lambda_{c,i}^{\text{local}} := [\lambda_{c,i}^{f_X},\ \lambda_{c,i}^{f_Y},\ \lambda_{c,i}^{f_Z},\ \lambda_{c,i}^{\tau_X},\ \lambda_{c,i}^{\tau_Y},\ \lambda_{c,i}^{\tau_Z}]^\top \in \mathbb{R}^6$ denotes the wrench vector in the local frame of the contact body. The CWC constraints are specified as follows:

$$\begin{gathered} |\lambda_{c,i}^{f_X}| \leq \mu\lambda_{c,i}^{f_Z}, \quad |\lambda_{c,i}^{f_Y}| \leq \mu\lambda_{c,i}^{f_Z}, \quad |\lambda_{c,i}^{\tau_X}| \leq L_X\lambda_{c,i}^{f_Z}, \\ \lambda_{c,i}^{\tau_Y}| \leq L_Y\lambda_{c,i}^{f_Z}, \quad \underline{\lambda}_{c,i}^{\tau_Z} \leq \lambda_{c,i}^{\tau_Z} \leq \overline{\lambda}_{c,i}^{\tau_Z}, \end{gathered} \tag{7}$$

where

$$\underline{\lambda}_{c,i}^{\tau_Z} = -\mu L_{XY}\lambda_{c,i}^{f_Z} + |L_Y\lambda_{c,i}^{f_X} - \mu\lambda_{c,i}^{\tau_X}| + |L_X\lambda_{c,i}^{f_Y} - \mu\lambda_{c,i}^{\tau_Y}|,$$

$$\overline{\lambda}_{c,i}^{\tau_Z} = \mu L_{XY}\lambda_{c,i}^{f_Z} - |L_Y\lambda_{c,i}^{f_X} + \mu\lambda_{c,i}^{\tau_X}| - |L_X\lambda_{c,i}^{f_Y} + \mu\lambda_{c,i}^{\tau_Y}|.$$

L_X, L_Y and μ denote the distance to the vertex from the center of the contact surface in X and Y direction and the friction coefficient, respectively, and $L_{XY} = L_X + L_Y$. Given a contact candidate $i \in \mathcal{I}_{m_k}$, we can express these constraints as inequality constraints as follows:

$$\mathcal{W}_i(x, \lambda_{c,i}) = \mathbf{C}_i \left[\begin{array}{cc} \mathbf{R}_{c,i}^\top(q) & \mathbf{0} \\ \mathbf{0} & \mathbf{R}_{c,i}^\top(q) \end{array} \right] \lambda_{c,i} \geq 0 \tag{8}$$

where $\mathbf{C}_i \in \mathbb{R}^{16\times6}$ is the matrix form of the wrench constants in (7). $\mathbf{R}_{c,i}(q)$ denotes the rotation matrix of the contact body indexed i in terms of the global frame.

D. Problem Statement

In this paper, we solve a constrained trajectory optimization problem for high-dimensional robotic systems whose motion and constraints are described in Section II-B and II-C. The problem is sub-divided into two tractable problems to be solved in an efficient way. The first problem is to check whether there exists at least one trajectory that will steer the robotic system to the planned next contact location in $\mathbb{R}^3$. This reachability test will be performed based on full-body dynamics of the robotic system. The second problem corresponds to an OCP that seeks for the control torque command that will minimize a certain quadratic performance index while strictly enforcing kinematic and dynamics constraints for the switching contact mode.

III. THE PROPOSED APPROACH

In this section, we briefly review the TVR planner proposed in [11] and show how to utilize the planning results generated by this planner in our proposed trajectory generation method. In particular, the TVR planner produces a reference for the next contact point, which may not be necessarily reachable. For this reason, we propose a method, which relies on forward and backward reachability analysis tools, to verify whether it is possible to move from the current mode to the next one.

A. Time-to-Velocity-Reversal (TVR) Planner

The TVR planner depends on the LIPM in which a height of CoM is enforced as a constant value:

$$\ddot{p} = \frac{g}{h}(p - \alpha) \tag{9}$$

where $p \in \mathbb{R}^2$, g, h, and $\alpha \in \mathbb{R}^2$ denote the position of CoM, the gravitational acceleration, the height of CoM, and the current contact location, respectively. Let us define a CoM state $x_p = [p^\top,\ \dot{p}^\top]^\top$. Suppose that the step duration T be constant and that the CoM state in k-th step, $x_{p,k}$ be given. Then, we can achieve the state equation as follows:

$$x_{p,k+1} = \mathbf{A}(T)x_{p,k} + \mathbf{B}(T)\alpha_k \tag{10}$$

where $x_{p,k+1}$ denotes the CoM state after the step duration T. The matrices $\mathbf{A}(T)$ and $\mathbf{B}(T)$ are specified such as

$$\mathbf{A}(T) = \left[\begin{array}{c} \mathbf{A}_p(T) \\ \hline \mathbf{A}_v(T) \end{array} \right] = \left[\begin{array}{cccc} \mathcal{C}(T) & 0 & \frac{\mathcal{S}(T)}{\omega} & 0 \\ 0 & \mathcal{C}(T) & 0 & \frac{\mathcal{S}(T)}{\omega} \\ \hline \omega\mathcal{S}(T) & 0 & \mathcal{C}(T) & 0 \\ 0 & \omega\mathcal{S}(T) & 0 & \mathcal{C}(T) \end{array} \right]$$

$$\mathbf{B}(T) = \left[\begin{array}{c} \mathbf{B}_p(T) \\ \hline \mathbf{B}_v(T) \end{array} \right] = \left[\begin{array}{cc} 1 - \mathcal{C}(T) & 0 \\ 0 & 1 - \mathcal{C}(T) \\ \hline -\omega\mathcal{S}(T) & 0 \\ 0 & -\omega\mathcal{S}(T) \end{array} \right]$$

where $\omega = \sqrt{g/h}$, $\mathcal{C}(t) = \cosh(\omega t)$, and $\mathcal{S}(t) = \sinh(\omega t)$. Assuming there exist reversal time, $t_s < T$, to make the CoM velocity becomes zero, that is, $\mathbf{A}_v(t_s)x_{p,k} + \mathbf{B}_v(t_s)\alpha_k = 0$, we compute the desired contact point, α_k^d, with bias terms, $\kappa_1, \kappa_2 \in \mathbb{R}$, as follows:

$$\begin{aligned} \alpha_k^d &= \mathbf{B}_v^\dagger(t_s)\mathbf{A}_v(t_s)x_{p,k} + \mathbf{\Phi}_\kappa x_{p,k}, \\ \mathbf{\Phi}_\kappa &= \left[\begin{array}{ccc} \kappa_1 & 0 & \mathbf{0}_{1\times2} \\ 0 & \kappa_2 & \mathbf{0}_{1\times2} \end{array} \right] \in \mathbb{R}^{2\times4}. \end{aligned} \tag{11}$$

The detailed explanation about the role of the bias term, κ, is presented in [11]. Substituting α_k^d in (11) to α_k in (10), we obtain the closed-loop state space dynamics of TVR planner:

$$x_{p,k+1} = (\mathbf{A}(T) + \mathbf{B}(T)\mathbf{K}(t_s))\, x_{p,k} \tag{12}$$

where $\mathbf{K}(t_s) = \mathbf{B}_v^\dagger(t_s)\mathbf{A}_v(t_s) + \mathbf{\Phi}_\kappa$. It is unclear whether the desired contact point α_k^d is achievable, because the planner ignores full-body dynamics and the constraints described in Section II-B and II-C. In addition, the planner merely determines the next contact point at the specific time instance thus the detailed trajectory needs to be generated using the interpolation methods [11], [14]. To overcome this disadvantage of the LIPM-based planning and simple interpolation, we propose further steps for checking the reachability and for generating a feasible trajectory by solving an OCP.

B. Kinematic Feasibility

Before we perform full-scale reachability analysis for the robotic system, we check whether the next contact location is kinematically feasible, assuming the current contact location does not move. Suppose that the planner produces the desired contact location, α_{k+1}^d, with respect to the current contact location, α_k, and the CoM state, $x_{p,k}$. Since we do not consider running and flying cases, the contact kinematics constraints (5) at both contact locations, α_k and α^d_{k+1}, should be fulfilled at time instance T; otherwise, the transition among the modes is infeasible. We cannot obtain a reachable path toward the next mode if the planned contact location is kinematically infeasible.

C. Reachable Sets

After checking that the contact location is feasible in a kinematic sense, we perform reachability analysis to check whether the next contact location is dynamically feasible underlying the dynamics and further constraints. To do so, let us define forward and backward reachable sets.

Definition 1. ***(Forward Reachable Set)*** *Suppose that the mode $m_k \in \mathcal{M}$ and the initial state x_0 are given. The forward reachable set (FWR) at time instance $t \geq t_0$ is defined as*

$$\begin{aligned}\overrightarrow{\mathcal{R}}(m_k, x_0, t) \coloneqq \{&x(t) : \text{constraints (5) with } m_k,\\ &h_{\text{state}}(x(\tau)) \leq 0,\ h_{\text{input}}(u(\tau)) \leq 0,\\ &\dot{x}(\tau) = f(x(\tau), u(\tau), m_k, \lambda_c(\tau))\\ &\mathcal{W}_i(x(\tau), \lambda_{c,i}(\tau)) \geq 0,\ \forall i \in \mathcal{I}_{m_k},\\ &x(t_0) = x_0,\ \forall \tau \in [t_0, t]\}.\end{aligned}$$

The defined FWR can be extended over the finite horizon $\mathbf{T} = [t_0, t_f]$ as $\overrightarrow{\mathcal{R}}(m_k, x_0, \mathbf{T}) \coloneqq \cup_{t\in\mathbf{T}} \overrightarrow{\mathcal{R}}(m_k, x_0, t)$.

Definition 2. ***(Backward Reachable Set)*** *Let us consider a mode $m_k \in \mathcal{M}$ and a final state x_f. The backward reachable set (BWR) at time instance $t \leq t_f$ is defined as*

$$\begin{aligned}\overleftarrow{\mathcal{R}}(m_k, x_f, t) \coloneqq \{&x(t) : \text{constraints (5) with } m_k,\\ &h_{\text{state}}(x(\tau)) \leq 0,\ h_{\text{input}}(u(\tau)) \leq 0,\\ &\dot{x}(\tau) = f(x(\tau), u(\tau), m_k, \lambda_c(\tau))\\ &\mathcal{W}_i(x(\tau), \lambda_{c,i}(\tau)) \geq 0,\ \forall i \in \mathcal{I}_{m_k},\\ &x(t_f) = x_f,\ \forall \tau \in [t, t_f]\}.\end{aligned}$$

The BWR over the finite time interval $\mathbf{T} = [t_0, t_f]$ is also defined as $\overleftarrow{\mathcal{R}}(m_k, x_f, \mathbf{T}) \coloneqq \cup_{t\in\mathbf{T}} \overleftarrow{\mathcal{R}}(m_k, x_f, t)$.

It is possible to create sets in the output space associated with the defined FWR and BWR such that

$$\begin{aligned}\overrightarrow{\mathcal{Y}}(m_k, x_0, \mathbf{T}) &\coloneqq \{f_y(x) : x \in \overrightarrow{\mathcal{R}}(m_k, x_0, \mathbf{T})\},\\ \overleftarrow{\mathcal{Y}}(m_k, x_f, \mathbf{T}) &\coloneqq \{f_y(x) : x \in \overleftarrow{\mathcal{R}}(m_k, x_f, \mathbf{T})\}.\end{aligned} \tag{13}$$

We consider set-value mappings $\overrightarrow{f}_y : \overrightarrow{\mathcal{R}}(m_k, x_0, \mathbf{T}) \rightrightarrows \overrightarrow{\mathcal{Y}}(m_k, x_0, \mathbf{T})$ and $\overleftarrow{f}_y : \overleftarrow{\mathcal{R}}(m_k, x_f, \mathbf{T}) \rightrightarrows \overleftarrow{\mathcal{Y}}(m_k, x_f, \mathbf{T})$, which are upper hemicontinuous. In addition, the output space is frequently lower dimensional than the state space in robotics applications. For this reason, it may be more intuitive to interpret the reachable sets in the output space than the reachability analysis in the state space. To do that, we utilize the Hausdorff distance [23] between two measurable sets $\mathcal{A}$ and $\mathcal{B}$[1], i.e.,

$$d_H(\mathcal{A}, \mathcal{B}) = \max\left\{\sup_{a\in\mathcal{A}} \inf_{b\in\mathcal{B}} d(a, b), \sup_{b\in\mathcal{B}} \inf_{a\in\mathcal{A}} d(a, b)\right\} \tag{14}$$

where $d(a, b) \coloneqq \|a - b\|$.

Proposition 1. *Suppose that a FWR, $\overrightarrow{\mathcal{R}}(m_k, x_0, \mathbf{T}_k)$, and a BWR, $\overleftarrow{\mathcal{R}}(m_k, x_f, \mathbf{T}_{k+1})$, are given compact sets where $\mathbf{T}_k = [t_i, t_1]$, $\mathbf{T}_{k+1} = [t_2, t_f]$, and $t_i \leq t_2 \leq t_1 \leq t_f$. In addition, $x_f \in \mathcal{X}_{m_{k+1}}$ where $\mathcal{X}_{m_{k+1}}$ represents the admissible set of states fulfilling the constraints associated with the mode m_{k+1}. There exist at least one path from x_0 to x_f with the mode change if $\overrightarrow{\mathcal{Y}}(m_k, x_0, \mathbf{T}_k) \cap \overleftarrow{\mathcal{Y}}(m_k, x_f, \mathbf{T}_{k+1}) \neq \emptyset$ or $d_H(\overrightarrow{\mathcal{Y}}(m_k, x_0, \mathbf{T}_k), \overleftarrow{\mathcal{Y}}(m_k, x_f, \mathbf{T}_{k+1})) = 0$.*

Proof: Suppose that there exist a feasible and connected path $\mathcal{P}([t_i, T])$ where $\mathcal{P}(t_i) = x_0$ and $\mathcal{P}(T) = x_f$, and $T \leq (t_f + t_1 - t_2)$. If $\overrightarrow{\mathcal{Y}}(m_k, x_0, \mathbf{T}_k) \cap \overleftarrow{\mathcal{Y}}(m_k, x_f, \mathbf{T}_{k+1}) = \emptyset$, the union of two sets $\overrightarrow{\mathcal{R}}(m_k, x_0, \mathbf{T}_k)$ and $\overleftarrow{\mathcal{R}}(m_k, x_f, \mathbf{T}_{k+1})$ do not form a connected set. Because all reachable sets are compact and connected, the inverse of continuous set mappings are also continuous in the closed sets. It implies that the path $\mathcal{P}([t_i, T])$ is not connected because two reachable sets in the state space are not connected. If the path $\mathcal{P}([t_i, T])$ is not connected, $\overrightarrow{\mathcal{R}}(m_k, x_0, \mathbf{T}_k) \cap \overleftarrow{\mathcal{R}}(m_k, x_f, \mathbf{T}_{k+1}) = \emptyset$. $d_H(\overrightarrow{\mathcal{Y}}(m_k, x_0, \mathbf{T}_k), \overleftarrow{\mathcal{Y}}(m_k, x_f, \mathbf{T}_{k+1})) = 0$ is a special case such that $\overrightarrow{\mathcal{Y}}(m_k, x_0, \mathbf{T}_k)$ and $\overleftarrow{\mathcal{Y}}(m_k, x_f, \mathbf{T}_{k+1})$ are same. Since the reachable sets are connected and contain both initial and final states, there exist at least one path. □

D. Reachability Analysis in Discrete Time Domain

In reality, the control loop of our robotic system is updated at a short time interval of Δt (1 ms). For this reason, we formulate a finite-dimensional convex optimization problem to obtain the state at next time step from the given initial state x_0 in a discrete-time sense. In this section, we describe two approaches that obtain FWR and BWR.

1) Approach for FWR: Suppose the current j-th state, $x_j = [q_j^\top,\ \dot{q}_j^\top]^\top$, the current mode, m_k, the index set of the contact bodies, $\mathcal{I}_{m_k}$, and time increment, Δt, are given. One way to propagate the state is to utilized random input samples generated considering the constrained range, which is to fulfill $h_{\text{input}}(u) \leq 0$. We draw a random input from a uniform distribution in $[\underline{u}_s,\ \overline{u}_s]$, that is $U_s \sim \mathcal{U}(\underline{u}_s, \overline{u}_s)$ for all $s \in \{1, \cdots, n_u\}$. Random input torque vectors are generated as $u = [u_1, \cdots, u_{n_u}]^\top \in \mathbb{R}^{n_u}$ where $u_s \in U_s$ for all $s \in \{1, \cdots, n_u\}$. Then, we formulate a simple convex optimization problem as follows:

$$\begin{aligned}\min_{\ddot{q}_j, \delta_u, \lambda_c} \quad & \|\ddot{q}_j\|^2_{\mathbf{W}_{\ddot{q}}} + \|\delta_u\|^2_{\mathbf{W}_u} + \sum_{i\in\mathcal{I}_{m_k}} \|\lambda_{c,i}\|^2_{\mathbf{W}_\lambda}\\ \text{s.t.} \quad & \dot{x}_j = f(x_j, u_j, m_k, \lambda_c),\\ & h_{\text{input}}(u_j) \leq 0,\ u_j = u + \delta u,\\ & h_{\text{state}}(x_{j+1}) \leq 0,\ \ddot{\phi}_i(q_j, \dot{q}_j, \ddot{q}_j) = 0,\\ & \mathcal{W}_i(x_j, \lambda_{c,i}) \geq 0,\ \forall i \in \mathcal{I}_{m_k}\end{aligned} \tag{15}$$

[1] All reachable sets defined in this paper are measurable and compact.

where $u_j, u \in \mathbf{U}$ is a set of inputs satisfying the input constraints, $\mathbf{U} := \{u \in \mathbb{R}^{n_u} : h_{\text{input}}(u) \leq 0, \forall u \in \mathbb{R}^{n_u}\}$. Using the optimal variable $\ddot{q}_j^\star$ from the problem (15), we are able to obtain the reachable set recursively updated:

$$\begin{aligned}\overrightarrow{\mathcal{R}}^D(m_k, x_0, t_{j+1}) = \{&x_{j+1} \in \mathbb{R}^{n_x} : \\ &x_{j+1} = \begin{bmatrix} q_{j+1} \\ \dot{q}_{j+1} \end{bmatrix} = \begin{bmatrix} q_j + \Delta t \dot{q}_j \\ \dot{q}_j + \Delta t \ddot{q}_j^\star \end{bmatrix}, \\ &\exists \ddot{q}_j^\star \text{ in (15)}, \forall x_j \in \overrightarrow{\mathcal{R}}^D(m_k, x_0, [t_0, t_j])\}\end{aligned} \tag{16}$$

where $t_{j+1} = t_j + \Delta t > t_j \geq t_0$ and $\overrightarrow{\mathcal{R}}^D(m_k, x_0, t_1) := \{x_1 : \dot{q}_1 = \dot{q}_0 + \Delta t \ddot{q}_0^\star,\ q_1 = q_0 + \Delta t \dot{q}_0\}$. Since x_0 is feasible, which means $\phi_k(q_0) = 0$ and $\dot{\phi}_k(q_0, \dot{q}_0) = 0$, and $\ddot{q}_0^\star$ fulfill $\ddot{\phi}_k(q_0, \dot{q}_0, \ddot{q}_0^\star) = 0$, the propagated states are also kinematically feasible if the discretized time interval Δt is small. In addition, it is straightforward that the propagated states satisfy the state, input, and CWC constraints as well due to $\ddot{q}_j^\star$ in (15).

2) Approach for BWR: The way to obtain BWR is more complicated than the forward reachability analysis because we need to perform backward propagation of the rigid body dynamics, which is not a convex optimization problem. Suppose that the j-th state, x_j, the index set of the contact bodies, $\mathcal{I}_{m_k}$, and backward time variation Δt be given. $\dot{q}_{j-1} = \dot{q}_j - \Delta t \ddot{q}$ and $q_{j-1} = q_j - \Delta t \dot{q}_j$ are considered as unknowns in the optimization problem. In contrast to (15), the robot dynamics with respect to q_{j-1} and $\dot{q}_{j-1}$ becomes nonlinear; therefore, we need to solve the optimization by NLP. It is well known that NLP techniques may require long computational times to find a solution. To resolve this issue, we simplify the optimization problem to a QP problem by deploying a sampling-based approach.

For the process of backward propagation, we draw a random sample of the joint velocity $\dot{q} \sim \mathcal{U}(\dot{q}_j - \Delta t \overline{\ddot{q}}, \dot{q}_j - \Delta t \underline{\ddot{q}})$ and suppose $\mathbf{Q}$ be a set of the generated random samples. We introduce a new variable v_j satisfying $\dot{\phi}_i(q_j, v_j) = 0$ and the variable can be obtained as follows[2]:

$$\begin{aligned} v_j &= \mathbf{N}_{\mathcal{I}_{m_k}}(q_j)\dot{q}, \quad \forall \dot{q} \in \mathbf{Q}, \\ \mathbf{N}_{\mathcal{I}_{m_k}}(q_j) &= \mathbf{I} - \widehat{\mathbf{J}}_{\mathcal{I}_{m_k}}^{\dagger \mathbf{M}^{-1}}(q_j)\widehat{\mathbf{J}}_{\mathcal{I}_{m_k}}(q_j), \end{aligned} \tag{17}$$

where $\widehat{\mathbf{J}}_{\mathcal{I}_{m_k}}(q) = \text{vertcat}(\mathbf{J}_{c,i}(q), \forall i \in \mathcal{I}_{m_k})$. Under the assumption that $\widehat{\mathbf{J}}_{\mathcal{I}_{m_k}}(q)$ is full rank, it is clear that

$$\dot{\phi}_i(q_j, v_j) = \mathbf{J}_{c,i}(q_j)v_j = \mathbf{J}_{c,i}(q_j)\mathbf{N}_{\mathcal{I}_{m_k}}(q_j)\dot{q} = 0 \tag{18}$$

since $\mathbf{J}_{c,i}(q_j)\mathbf{N}_{\mathcal{I}_{m_k}}(q_j) = \mathbf{0}$ for all $i \in \mathcal{I}_{m_k}$. The projected velocity, v_j, is utilized to compute the state in $j-1$ step: $\dot{q}_{j-1} = \dot{q}_j - v_j$ and $q_{j-1} = q_j - \Delta t \dot{q}_j$. If the j-th state x_j is kinematically feasible, $\phi_i(q_j) = 0$, and $\dot{\phi}_i(q_j, \dot{q}_j) = 0$, we approximate $\phi_i(q_{j-1})$ by neglecting high order terms as follows:

$$\phi_i(q_{j-1}) = \phi_i(q_j) - \Delta t \mathbf{J}_{c,i}(q_j)\dot{q}_j + \mathcal{O}(|\Delta t|^2) \approx 0$$

with sufficiently small Δt. The derivative of $\phi_i(q_{j-1})$ is also approximated as follows:

$$\begin{aligned}\dot{\phi}_i(q_{j-1}, \dot{q}_{j-1}) =& \dot{\phi}_i(q_j, \dot{q}_j) - \Delta t \frac{\partial}{\partial q}\dot{\phi}_i(q_j, \dot{q}_j)\dot{q}_j \\ &- \frac{\partial}{\partial \dot{q}}\dot{\phi}_i(q_j, \dot{q}_j)v_j + \mathcal{O}(|\Delta t|^2) \approx 0.\end{aligned}$$

Since the second term of the derivative of $\phi_i(q_{j-1})$ is 0 with condition $\ddot{\phi}_i(q_j, \dot{q}_j, \ddot{q}_j) = 0$, the derivative of $\phi_i(q_{j-1})$ is also approximated as 0 by neglecting higher order terms. These two approximations enable that the updated states are kinematically feasible.

Using x_{j-1}, we check whether the state fulfills the state constraint: $h_{\text{state}}(x_{j-1}) \leq 0$. If the propagated state satisfies the constraints, we try to find appropriate control input and contact forces as follows:

$$\begin{aligned} \text{find} \quad & u,\ \lambda_c \\ \text{s.t.} \quad & \dot{x}_{j-1} = f(x_{j-1}, u, m_k, \lambda_c), \\ & h_{\text{input}}(u) \leq 0, \\ & \mathcal{W}_i(x_j, \lambda_{c,i}) \geq 0,\ \forall i \in \mathcal{I}_{m_k}. \end{aligned} \tag{19}$$

If there exist optimal decision variables $u^\star$ and $\lambda_c^\star$, we consider the state x_{j-1} as an element of BWR in the same way to the FWR, otherwise, the propagated state is discarded. BWR is obtained by recursively solving the optimization problem (19):

$$\begin{aligned}\overleftarrow{\mathcal{R}}^D(m_k, x_f, t_{j-1}) = \{&x_{j-1} \in \mathbb{R}^{n_x} : \\ &x_{j-1} = \begin{bmatrix} q_{j-1} \\ \dot{q}_{j-1} \end{bmatrix} = \begin{bmatrix} q_j - \Delta t \dot{q}_j \\ \dot{q}_j - v_j^\star \end{bmatrix}, \\ &\exists u^\star \text{ in (19)}, \forall x_j \in \overleftarrow{\mathcal{R}}^D(m_k, x_f, [t_j, t_f])\}\end{aligned} \tag{20}$$

where $t_{j-1} = t_j - \Delta t < t_j \leq t_f$ and $v_j^\star$ denotes the projected velocity onto the null-space $\mathbf{N}_{\mathcal{I}_{m_k}}$, which produces optimal decision variables in (19). Given a feasible final state x_f, we can obtain $\overleftarrow{\mathcal{R}}^D(m_k, x_f, t_{f-1}) = \left\{x_{f-1} : \dot{q}_{f-1} = \dot{q}_f - v_f^\star,\ q_{f-1} = q_f - \Delta t \dot{q}_f\right\}$. From this set, it is possible to recursively expand our reachable set backward over a finite time horizon without NLP.

3) Boundary Samples Propagation: Since the number of QPs required for obtaining reachable sets exponentially increases with respect to the number of time steps, the reachability analysis for longer time horizons imposes heavier computation burden as proved in [21]. For the sake of computational efficiency of the algorithms, we reduce the number of samples to be updated when computing $\overrightarrow{\mathcal{R}}^D(m_k, x_0, \mathbf{T}_k)$ in (16) and $\overleftarrow{\mathcal{R}}^D(m_k, x_f, \mathbf{T}_k)$ in (20). We utilized the method to select the boundary samples in the output space proposed in [8], [21]. Instead of considering all samples, we propagate the state samples at the boundary of the reachable set in the previous time step. Let suppose a set $\mathcal{A} \subseteq \mathbb{R}^{n_x}$ and a set-value mapping $\widetilde{f}_y : \mathcal{A} \rightrightarrows \mathcal{B} \subseteq \mathbb{R}^{n_y}$, e.g, $\overrightarrow{f}_y$ and $\overleftarrow{f}_y$, be given. The set of boundary state samples under $\widetilde{f}_y$, which is a subset of $\mathcal{A}$, is defined as follows:

$$\mathcal{A}^{\odot \widetilde{f}_y} := \{x \in \mathbb{R}^{n_x} : \widetilde{f}_y(x) \in \text{bd}(\mathcal{B}), \forall x \in \mathcal{A}\} \tag{21}$$

[2] Alternatively, the weighting matrix $\mathbf{M}^{-1}$ can be replaced to the identity matrix $\mathbf{I}$ with the same dimension of $\mathbf{M}^{-1}$. It changes the different weighting effects on the cost function of the least-square problem.

where $\mathrm{bd}(\mathcal{B})$ denotes the topological boundary set of $\mathcal{B}$, i.e., $\mathrm{bd}(\mathcal{B}) \subset \mathcal{B}$. We replace $\overrightarrow{\mathcal{R}}^D(m_k, x_0, [t_0, t_j])$ and $\overleftarrow{\mathcal{R}}^D(m_k, x_f, [t_j, t_f])$ to $(\overrightarrow{\mathcal{R}}^D(m_k, x_0, [t_0, t_j]))^{\odot \overrightarrow{f}_y}$ and $(\overleftarrow{\mathcal{R}}^D(m_k, x_f, [t_j, t_f]))^{\odot \overleftarrow{f}_y}$ in (16) and (20), respectively. Then, we can reduce the number of QPs required for obtaining the reachable sets, which improve the computational efficiency of the proposed approach.

4) Connectivity of Two Sets in Discrete Time Domain: Since discretizing the problem and the process obtaining the reachable sets, we need to prove the connectivity of two reachable sets in discrete time domain.

Proposition 2. *Let suppose that $\overrightarrow{\mathcal{R}}^D(m_k, x_0, \mathbf{T}_k) \subseteq \overrightarrow{\mathcal{R}}(m_k, x_0, \mathbf{T}_k)$ and $\overleftarrow{\mathcal{R}}^D(m_k, x_f, \mathbf{T}_{k+1}) \subseteq \overleftarrow{\mathcal{R}}(m_k, x_f, \mathbf{T}_{k+1})$ are given with the same time specification to those, in addition, $x_f \in \mathcal{X}_{m_{k+1}}$ such as Proposition 1. Δt is the time step for the discretization. There exist a path from x_0 to x_f iff*

$$d_H(\overrightarrow{\mathcal{Y}}^D(m_k, x_0, \mathbf{T}_k), \overleftarrow{\mathcal{Y}}^D(m_k, x_f, \mathbf{T}_{k+1})) \leq \delta$$

where $0 \leq \delta \leq K$. The bound K is defined as $K := \min\left\{\mathcal{K}(\overrightarrow{\mathcal{Y}}^D(m_k, x_0, \mathbf{T}_k)), \mathcal{K}(\overleftarrow{\mathcal{Y}}^D(m_k, x_f, \mathbf{T}_{k+1}))\right\}$ by comparing the Hausdorff distance as follows: $\mathcal{K}(\mathcal{A}) = \max_{a \in \mathcal{A}} d_H(\{a\}, \mathcal{A} \backslash \{a\})$.

Proof: We prove the proposition by using the Lipschitz continuity of the dynamics functions with two modes m_k and m_{k+1}. There exist two Lipschitz constants, $\mathcal{L}_k \geq 0$ and $\mathcal{L}_{k+1} \geq 0$, satisfying $d(f_k(a_1, u_{a_1}), f_k(a_2, u_{a_2})) \leq \mathcal{L}_k(d(a_1, a_2) + d(u_{a_1}, u_{a_2}))$ and $d(f_{k+1}(b_1, u_{b_1}), f_{k+1}(b_2, u_{b_2})) \leq \mathcal{L}_{k+1}(d(b_1, b_2) + d(u_{b_1}, u_{b_2}))$ where $u_{a_1}, u_{a_2}, u_{b_1}, u_{b_2} \in \mathbf{U}$, $a_1, a_2 \in \overrightarrow{\mathcal{R}}^D(m_k, x_0, \mathbf{T}_k)$ and $b_1, b_2 \in \overleftarrow{\mathcal{R}}^D(m_k, x_f, \mathbf{T}_{k+1}) \cap \mathcal{X}_{m_{k+1}}$, respectively. Let us consider $\gamma = d(f_k(a_2, u_{a_2}), f_{k+1}(b_1, u_{b_1}))$ then $d(f_k(a_1, u_{a_1}), f_{k+1}(b_2, u_{b_2})) \leq \mathcal{L}_k(d(a_1, a_2) + d(u_{a_1}, u_{a_2})) + \mathcal{L}_{k+1}(d(b_1, b_2) + d(u_{b_1}, u_{b_2})) + \gamma$. Suppose there exists an injective and continuous mapping $f_{y'} : \mathbb{R}^{n_x} \mapsto \mathbb{R}^{n_x}$ for which the first n_y elements form a vector that is equal to $f_y(x)$ and the remaining components correspond to a vector that belongs to the null-space of $f_y(x)$, which is a subspace of $\mathbb{R}^{n_x - n_y}$. Then, $f_{y'}$ is bi-Lipschitz continuous, which means $\mathcal{L}_{y'}^{-1} d(a_1, a_2) \leq d(f_{y'}(a_1), f_{y'}(a_2)) \leq \mathcal{L}_{y'} d(a_1, a_2)$ if there exists a $\mathcal{L}_{y'} > 1$. Since $d(f_{y'}(a_1), f_{y'}(a_2)) \leq d(f_y(a_1), f_y(a_2)) + d(a_1, a_2)$ and $d(f_y(a_1), f_y(a_2)) \leq \delta$, $d(a_1, a_2) \leq \mathcal{L}_y \delta$ and $d(b_1, b_2) \leq \mathcal{L}_y \delta$ where $\mathcal{L}_y = (\mathcal{L}_{y'}^{-1} - 1)^{-1}$. Since there exist inputs $u_{a_1} = u_{a_2}$, $u_{b_1} = u_{b_2}$, and constant $\mathcal{L}$ satisfying $d(f_k(a_1, u_{a_1}), f_{k+1}(b_2, u_{b_2})) \leq (\mathcal{L}_k + \mathcal{L}_{k+1})\mathcal{L}_y \delta + \gamma \leq \mathcal{L}(d(a_1, b_2) + d(u_{a_1}, u_{b_2}))$. Therefore, we have shown there exists a bounded and connected from (a_1, u_{a_1}) to (b_2, u_{b_2}). □

E. Optimal Control for Trajectory Generation

If the planned contact location turns out to be reachable via the proposed approach, then we proceed with the formulation of an optimal control problem (OCP) whose solution will correspond to the state trajectory that will take the system to the planned location. Given the predetermined parameters, x_0, x_f, t_0, t_1, t_2, and t_f where $t_0 < t_2 \leq t_1 < t_f$, we perform reachability analysis to obtain FWR and BWR, $\overrightarrow{\mathcal{R}}^D(m_k, x_0, [t_0, t_1])$ and $\overleftarrow{\mathcal{R}}^D(m_k, x_f, [t_2, t_f])$ where $x_f \in \mathcal{X}_{m_{k+1}}$. Then, let us denote the union of the two sets as $\overleftrightarrow{\mathcal{R}}^D(m_k, x_0, x_f, [t_0, t_f]) := \overrightarrow{\mathcal{R}}^D(m_k, x_0, [t_0, t_1]) \cup \overleftarrow{\mathcal{R}}^D(m_k, x_f, [t_2, t_f])$. To formulate the OCP, we define a performance measure in the discrete time domain:

$$\begin{aligned} \mathcal{G}(\mathbf{u}, N) := \sum_{j=0}^{N} \{ & u^\top(t_j)\mathbf{Q}_u u(t_j) + \lambda_c^\top(t_j)\mathbf{Q}_\lambda \lambda_c(t_j) \\ & + (x(t_j) - x_f)^\top \mathbf{Q}_x (x(t_j) - x_f) \} \end{aligned} \tag{22}$$

where $\mathbf{u} := \{u(t_0), u(t_1), \ldots, u(t_N)\}$, e.g., $t_N = t_f$, and N is the number of time steps from t_0 to t_f in the time interval Δt. In addition, $\mathbf{Q}_u \in \mathbb{S}_{>0}^{n_u}$, $\mathbf{Q}_\lambda \in \mathbb{S}_{>0}^{\dim \lambda_c}$, and $\mathbf{Q}_x \in \mathbb{S}_{\geq 0}^{n_x}$ are the weighting matrices for each term of the performance measure, respectively. When the next contact location is reachable in accordance with Proposition 1 or 2, then we formulate the OCP as follows:

$$\begin{aligned} \min_{\mathbf{\Psi}, \mathbf{u}, \mathbf{\Lambda}} \quad & \mathcal{G}(\mathbf{u}, N) \\ \text{s.t.} \quad & \dot{\xi}(t_j) = f(\xi(t_j), u(t_j), m_k, \lambda_c(t_j)), \\ & \xi(t_j) \in \overleftrightarrow{\mathcal{R}}^D(m_k, x_0, x_f, [t_0, t_f]), \\ & \ddot{\phi}_{i_1}(\dot{\xi}(t_j), \xi(t_j)) = 0,\ \forall i_1 \in \mathcal{I}_{m_k}, \\ & \mathcal{W}_{i_1}(\xi(t_j), \lambda_{c,i_1}(t_j)) \geq 0,\ \forall i_1 \in \mathcal{I}_{m_k}, \\ & \phi_{i_2}(\xi(t_f)) = 0,\ \dot{\phi}_{i_2}(\xi(t_f)) = 0, \\ & \ddot{\phi}_{i_2}(\dot{\xi}(t_f), \xi(t_f)) = 0,\ \forall i_2 \in \mathcal{I}_{m_{k+1}}, \\ & \mathcal{W}_{i_2}(\xi(t_f), \lambda_{c,i_2}(t_f)) \geq 0,\ \forall i_2 \in \mathcal{I}_{m_{k+1}}, \\ & h_{\text{input}}(u(t_j)) \leq 0,\ t_0 \leq t_j \leq t_f, \\ & x(t_0) = x_0,\ x(t_f) = x_f \end{aligned} \tag{23}$$

where $\mathbf{\Psi} := \{\xi(t_0), \ldots, \xi(t_N)\}$ and $\xi(t) \in \mathbb{R}^{n_x}$. In addition, $\mathbf{u} := \{u(t_0),\ \cdots,\ u(t_N)\}$ and $\mathbf{\Lambda} := \{\lambda_c(t_0),\ \cdots, \lambda_c(t_N)\}$. If the Proposition 1 or 2 are satisfied, there exist a optimal solution of the formulated OCP. If the contact point is infeasible, we relax the hard constraint $x(t_f) = x_f$ and some part of $\phi_{i_2}(\xi(t_f)) = 0$, more specifically, by modifying $\phi_{i_2}(\xi(t_f)) - \varepsilon_{i_2} = 0$ where $\varepsilon_{i_2} = \left[\epsilon_{i_2}^X,\ \epsilon_{i_2}^Y,\ 0,\ 0,\ 0,\ 0\right]^\top \in \mathbb{R}^6$. $\epsilon_{i_2}^X$ and $\epsilon_{i_2}^Y$ are optimal decision variables to be minimized so that we have to include the quadratic terms for these relaxed variables in the cost function. Then, we can find an alternative trajectory to reach the closest point to the planned contact location.

IV. NUMERICAL SIMULATIONS

In this section, we present numerical simulations to validate the proposed approach. For these simulations, we use a bipedal humanoid robot, i.e., *Valkyrie* in Fig 1(a), in the DART simulation environments [24]. *QuadProg++*, which is based on Goldfarb-Idinani active-set dual method, is utilized to solve QP problems and we solve NLP problems using

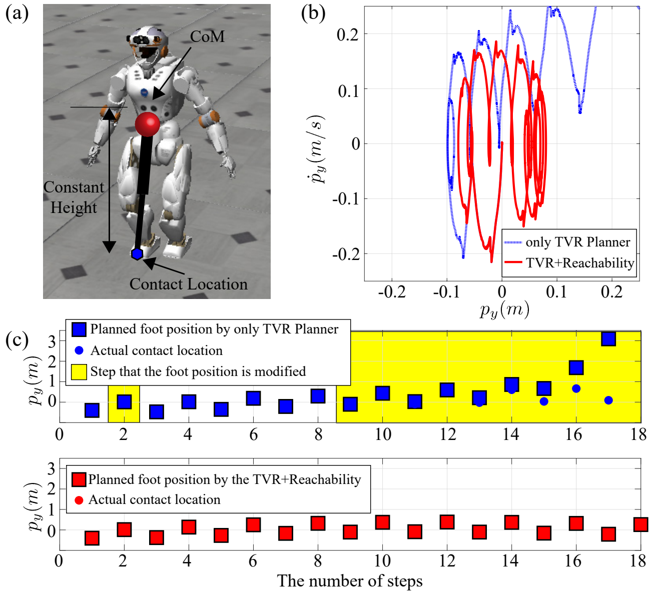

Fig. 1. Simulation Model and Planning Results:(a) Valkyrie simulation model and LIPM, (b) Phase space plot of CoM behaviors in Y direction, (c) Planned and actual contact locations.

IPOPT for the simulations[3]. Some interfaces of these simulations are supported by the *PnC* package[4] and MATLAB. As simulation scenarios, we implement stepping motions and compare the numerical simulation results with and without the proposed approach. The predefined contact sequence is to repeat (Double Support)→(Single Support: Left)→(Double Support)→(Single Support: Right)→(Double Support)→ $\cdots$ without considering the flying and running modes. We employ WBC in [14] and modify it to suit our needs in this simulations.

A. The TVR Planner with Heuristic Bounds

We utilize the TVR planner to provide the next contact location of the humanoid robot. We set up several heuristic parameters for the planner: $t_s = 0.15$, $\kappa_{1,2} = -0.66$, $y^X_{\text{foot,limit}} = [-0.42,\ 0.42]$, $y^Y_{\text{foot,limit}} = [0.25,\ 0.65]$, and $\dot{p}_{\text{limit}} = [0.0,\ 1.3]$. In particular, the bounds $y^{X,Y}_{\text{foot,limit}}$ and $\dot{p}_{\text{limit}}$ are utilized to prevent big steps which cannot be achieved by the robot. The upper plot of Fig 1(c) presents the planned contact locations, actual contact points, and the steps modified by the bounds, which are marked as yellow regions. These modified contact locations perturb the CoM behavior depicted as a blue dotted line in Fig 1(b). Fig 2(a) shows the simulation results that the robot falls down. We recognize the discrepancy between the planned location (red pentagons) and the actual contact location (blue pentagons) due to the bounds (orange polygons).

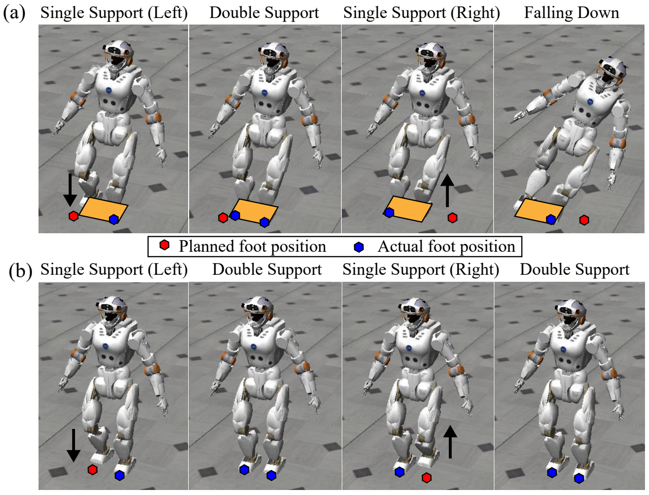

Fig. 2. Snapshots of the Simulations: (a) Stepping motions by the method only using the TVR planner with heuristic bounds, (b) Stepping motions by the proposed approach.

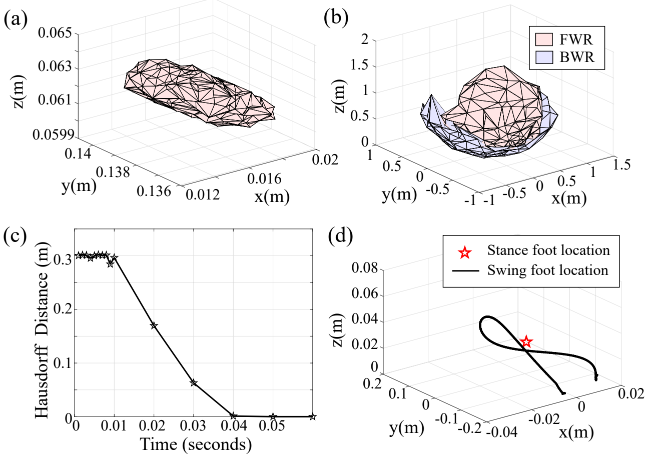

Fig. 3. Reachable sets and Hausdorff distance: (a) Samples of FWR and the corresponding boundary at $t = 0.003$ (seconds), (b) The boundaries of FWR and BWR at $t = 0.04$ (seconds), (c) The Hausdorff distance between FWR and BWR with respect to the finite time horizon, (d) The contact location of the stance foot and the position trajectory of the swing foot.

B. The Proposed Method with Reachable Sets

In this simulation scenario, we quickly test whether the planned contact location is reachable by using our reachability analysis method. The heuristic bounds utilized in Section IV-A are not required due to the reachability analysis. Fig 3 represents the results of reachability analysis for a single step, which is the transition (Single Support: Left)→(Double Support). We generate 1.0×10^4 samples in the first time step and keep propagating the states forward and backward by using the proposed methods. Consider $t = 0$ (seconds) when the planner generate the next contact location. Fig 3(a) shows the FWR and its boundary for the right-side foot at $t = 0.003$ (seconds). Fig 3(b) presents the FWR and BWR at $t = 0.4$ (seconds) obtained by the proposed method. We check that the Hausdorff distance between the FWR and BWR is smaller than the threshold $\delta = 1.0 \times 10^{-5}$ at $t = 0.4$

[3] QuadProg++ Repository: https://github.com/liuq/QuadProgpp, IPOPT Repository: https://github.com/coin-or/Ipopt
[4] PnC Repository: https://github.com/junhyeokahn/PnC

(seconds), which is much smaller than the transition time t_s, as shown in Fig 3(c). Fig 3(d) presents the trajectory of the swing foot and the contact location of the stance foot. Our robot does not fall down and keeps walking as described in the snapshots of Fig 2(b). In addition, we verify that the planned contact locations are precisely tracked by the generated trajectories, as shown in the lower plot of Fig 1(c).

V. CONCLUSION

This paper proposes an approach to generate feasible state trajectories for a high-dimensional robotic system subject to contact constraints which is required to reach the next contact location planned by a simplified model-based planner. To the best our knowledge, this paper is the first one to integrate the TVR planner and reachability-based trajectory optimization considering full-body dynamics and attain the guaranteed trajectory to reach the planned location. In addition, a proposed algorithm performs reachability analysis in a more computationally efficient way than our previous work. In our approach, we compute the reachable sets by employing a sampling-based method that allows us to solve multiple QPs instead of solving high-dimensional and computationally intractable NLPs. In addition, the bi-directional propagation for the reachability analysis contributes to the reduction of computation time.

Our problem is still computationally expensive to be solved in real-time. This is because our approach relies on the solutions of multiple optimization problems subject to full-body dynamics and our robotic systems correspond to high-dimensional systems such as humanoid robots. Consequently, we cannot generate the trajectory in the real-time feedback loops. In the near future, we will investigate more efficient sampling-based methods to improve computational efficiency with a precise analysis of the computational complexity. Also, we will propose a method to generate optimal sequences of rigid contacts by utilizing the reachability analysis tools and full-body dynamics of robots.

ACKNOWLEDGMENT

The authors would like to thank the members of the Human Centered Robotics Laboratory at The University of Texas at Austin for their great help and support.

REFERENCES

[1] J. W. Grizzle, C. Chevallereau, A. D. Ames, and R. W. Sinnet, "3D bipedal robotic walking: models, feedback control, and open problems," *IFAC Proceedings Volumes*, vol. 43, no. 14, pp. 505–532, 2010.

[2] Y. Zhao, B. R. Fernandez, and L. Sentis, "Robust optimal planning and control of non-periodic bipedal locomotion with a centroidal momentum model," *International Journal of Robotics Research*, vol. 36, no. 11, pp. 1211–1242, 2017.

[3] D. Heck, A. Saccon, N. Van de Wouw, and H. Nijmeijer, "Guaranteeing stable tracking of hybrid position–force trajectories for a robot manipulator interacting with a stiff environment," *Automatica*, vol. 63, pp. 235–247, 2016.

[4] J. Carius, R. Ranftl, V. Koltun, and M. Hutter, "Trajectory optimization with implicit hard contacts," *IEEE Robotics and Automation Letters*, vol. 3, no. 4, pp. 3316–3323, Oct 2018.

[5] A. . nol, P. Long, and T. Padr, "Contact-implicit trajectory optimization based on a variable smooth contact model and successive convexification," in *Proceedings of the IEEE International Conference on Robotics and Automation*, May 2019, pp. 2447–2453.

[6] M. Neunert, M. Stäuble, M. Giftthaler, C. D. Bellicoso, J. Carius, C. Gehring, M. Hutter, and J. Buchli, "Whole-body nonlinear model predictive control through contacts for quadrupeds," *IEEE Robotics and Automation Letters*, vol. 3, no. 3, pp. 1458–1465, 2018.

[7] M. Posa, C. Cantu, and R. Tedrake, "A direct method for trajectory optimization of rigid bodies through contact," *International Journal of Robotics Research*, vol. 33, no. 1, pp. 69–81, 2014.

[8] J. Lee, E. Bakolas, and L. Sentis, "Trajectory generation for robotic systems with contact force constraints," in *Proceedings of the American Control Conference*, July 2019, pp. 671–678.

[9] T. Sugihara, Y. Nakamura, and H. Inoue, "Real-time humanoid motion generation through ZMP manipulation based on inverted pendulum control," in *Proceedings of the IEEE International Conference on Robotics and Automation*, vol. 2, 2002, pp. 1404–1409.

[10] N. Motoi, T. Suzuki, and K. Ohnishi, "A bipedal locomotion planning based on virtual linear inverted pendulum mode," *IEEE Transactions on Industrial Electronics*, vol. 56, no. 1, pp. 54–61, 2008.

[11] D. Kim, Y. Zhao, G. Thomas, B. R. Fernandez, and L. Sentis, "Stabilizing series-elastic point-foot bipeds using whole-body operational space control," *IEEE Transactions on Robotics*, vol. 32, no. 6, pp. 1362–1379, 2016.

[12] H. Dai, A. Valenzuela, and R. Tedrake, "Whole-body motion planning with centroidal dynamics and full kinematics," in *Proceedings of the IEEE-RAS/RSJ International Conference on Humanoid Robots*, 2014, pp. 295–302.

[13] B. Aceituno-Cabezas, C. Mastalli, H. Dai, M. Focchi, A. Radulescu, D. G. Caldwell, J. Cappelletto, J. C. Grieco, G. Fernández-López, and C. Semini, "Simultaneous contact, gait, and motion planning for robust multilegged locomotion via mixed-integer convex optimization," *IEEE Robotics and Automation Letters*, vol. 3, no. 3, pp. 2531–2538, 2017.

[14] D. Kim, S. Jorgensen, J. Lee, J. Ahn, J. Luo, and L. Sentis, "Dynamic locomotion for passive-ankle biped robots and humanoids using whole-body locomotion control," *arXiv preprint arXiv:1901.08100*, 2019.

[15] M. Althoff, O. Stursberg, and M. Buss, "Reachability analysis of nonlinear systems with uncertain parameters using conservative linearization," in *Proceedings of the IEEE Conference on Decision and Control*, 2008, pp. 4042–4048.

[16] M. Althoff and G. Frehse, "Combining zonotopes and support functions for efficient reachability analysis of linear systems," in *Proceedings of the IEEE Conference on Decision and Control*, 2016, pp. 7439–7446.

[17] I. M. Mitchell, A. M. Bayen, and C. J. Tomlin, "A time-dependent Hamilton-Jacobi formulation of reachable sets for continuous dynamic games," *IEEE Transactions on Automatic Control*, vol. 50, no. 7, pp. 947–957, 2005.

[18] S. Bansal, M. Chen, S. Herbert, and C. J. Tomlin, "Hamilton-Jacobi reachability: A brief overview and recent advances," in *Proceedings of the IEEE Conference on Decision and Control*, 2017, pp. 2242–2253.

[19] M. Oishi, I. Mitchell, C. Tomlin, and P. Saint-Pierre, "Computing viable sets and reachable sets to design feedback linearizing control laws under saturation," in *Proceedings of the IEEE Conference on Decision and Control*, 2006, pp. 3801–3807.

[20] L. Liebenwein, C. Baykal, I. Gilitschenski, S. Karaman, and D. Rus, "Sampling-based approximation algorithms for reachability analysis with provable guarantees," in *Proceedings of Robotics: Science and Systems*, Pittsburgh, Pennsylvania, June 2018.

[21] J. Lee, E. Bakolas, and L. Sentis, "Efficient trajectory generation for robotic systems constrained by contact forces," *arXiv preprint arXiv:1903.11163*, 2019.

[22] S. Caron, Q. Pham, and Y. Nakamura, "Stability of surface contacts for humanoid robots: Closed-form formulae of the contact wrench cone for rectangular support areas," in *Proceedings of the IEEE International Conference on Robotics and Automation*, May 2015, pp. 5107–5112.

[23] J. Munkres, *Topology*. Pearson Education, 2014.

[24] J. Lee, M. X. Grey, S. Ha, T. Kunz, S. Jain, Y. Ye, S. S. Srinivasa, M. Stilman, and C. K. Liu, "DART: dynamic animation and robotics toolkit." *J. Open Source Software*, vol. 3, no. 22, p. 500, 2018.